Local Avalanche Effect of 4H-SiC p-i-n Ultraviolet Photodiodes With Periodic Micro-Hole Arrays

Zhao Fu, Mingkun Zhang, Shan Han, Jiafa Cai, Rongdun Hong, Xiaping Chen, Dingqu Lin, Shaoxiong Wu, Yuning Zhang, Deyi Fu, Zhengyun Wu, Baoping Zhang, Feng Zhang, *Member, IEEE*, and Rong Zhang

***Abstract*—In this report, 4H-SiC p-i-n photodiodes with various micro-hole arrays are fabricated, then measured and discussed by using photoelectric measurement system and simulation software. Periodic micro-hole arrays etched from p layer to i layer are obtained by using the selective etching technology, which increases the photosensitive area of devices and reduces the ultraviolet light absorption of p layer. The average dark current of devices has an ultralow value of approximate 6.0 $\times$ 10^{-15} A in the low reverse bias range of 0-10 V. Furthermore, the device with 4 μm micro-hole exhibits the best performance and its peak responsivity increased by 10.4 % compared to the conventional device. It is significant that the peak responsivity and corresponding external quantum efficiency of devices with 4 μm micro-hole at 40 V bias are 815 % and 819 % higher than those of devices without micro-hole, respectively. This is attribute to the fact that a high electric field is observed around the micro-holes as the reverse bias increased to 40 V, which leads to local avalanche. Thus, the local avalanche photodiodes work at a relatively low bias, which improved the responsivity and quantum efficiency of the device enormously.**

***Index Terms*—4H-SiC, ultraviolet, photodiodes, micro-hole.**

I. Introduction

ULTRAVIOLET (UV) photodiodes (PDs) have attracted much attention owing to their extensive applications such as environmental monitoring, space science, UV communication and biological agent detection [1]–[3]. Taking advantages of its large bandgap energy, superior thermal conductivity, and high electron saturation velocity, SiC performs as an attractive candidate material to fabricate solar-blind PDs [4]. SiC UV PDs with various structures, such as schottky, p-i-n, metal-semiconductor-metal (MSM), and avalanche, have been developed to satisfy all kinds of applications [5]–[9].

However, the responsivity of SiC-based PDs is still lower than expected and need to be improved for weak UV signals detection. In recent years, many methods have been proposed to improve the performance of UV PDs. For instance, microlens arrays were fabricated on the SiC PDs to enhance the absorption efficiency of light [10]–[12]. The thinner p layer was also used to improve the spectral response of SiC p-i-n UV PDs [13]. Porous structure etched on the device surface by electrochemical method enhanced the surface roughness and reduced light reflection [14]–[16]. The nanohole and nanorod arrays were also used to improve the performance of the detectors owing to their light trapping [17], [18]. However, fabrication of microlens is a complex process and its cost is expensive. Electrochemical etching will increase the dark current of the device, and the size of pores is difficult to control. The micro-hole array structure is also a feasible method, which has been applied in solar cells to improve light absorption [19], [20].

In this work, 4H-SiC p-i-n UV PDs with periodic micro-hole arrays are fabricated. The effects of micro-hole arrays with various diameters on the performance of 4H-SiC PDs are discussed in detail by photoelectric measurements and Technology Computer Aided Design (TCAD) simulation.

II. Device Structure and Fabrication

Fig.1 (a) shows the schematic diagram of the 4H-SiC device with micro-hole arrays. The 4H-SiC epitaxial structure consists of a 200-nm-thick p^+ layer ($N_A = 1 \times 10^{19}$ cm^{-3}), a 3000-nm-thick i layer ($N_D = 1 \times 10^{15}$ cm^{-3}) and a 500-nm-thick n layer ($N_D = 2 \times 10^{18}$ cm^{-3}). Fig. 1(b) shows the top-view photograph of fabricated micro-hole array with p electrode. The photoactive window area of the detector is 200 $\times$ 200 μm^2. Prior to device fabrication, TCAD simulation are performed to analyze the influence of micro-hole on device performance. The devices are simulated using a plane 2-D structure, and the thickness and doping concentration are confirmed with the Fig. 1(a). TCAD solves the continuity and Poisson's equation for the charge carriers [21]. The default parameters are used for the concentration-dependent

Manuscript received November 20, 2021; accepted November 29, 2021. Date of publication December 3, 2021; date of current version December 29, 2021. This work was supported in part by the Fundamental Research Funds for the Central Universities under Grant 20720190049 and Grant 20720190053, in part by the Natural Science Foundation of Fujian Province of China for Distinguished Young Scholars under Grant 2020J06002, in part by the Science and Technology Project of Fujian Province of China under Grant 2020I0001, and in part by the Science and Technology Key Projects of Xiamen under Grant 3502ZCQ20191001. The review of this letter was arranged by Editor T.-Y. Seong. *(Corresponding authors: Mingkun Zhang; Feng Zhang; Rong Zhang.)*

Zhao Fu, Shan Han, Jiafa Cai, Rongdun Hong, Xiaping Chen, Dingqu Lin, Shaoxiong Wu, Yuning Zhang, Deyi Fu, Zhengyun Wu, and Feng Zhang are with the Department of Physics, College of Physical Science and Technology, Xiamen University, Xiamen 361005, China (e-mail: fzhang@xmu.edu.cn).

Mingkun Zhang is with the Department of Physics, College of Physical Science and Technology, and the School of Electronic Science and Engineering, Xiamen University, Xiamen 361005, China (e-mail: mkzhang@xmu.edu.cn).

Baoping Zhang is with the School of Electronic Science and Engineering, Xiamen University, Xiamen 361005, China.

Rong Zhang is with the Department of Physics, College of Physical Science and Technology, Xiamen University, Xiamen 361005, China, and also with the School of Electronic Science and Engineering, Nanjing University, Nanjing 210093, China (e-mail: rzhangxmu@xmu.edu.cn).

Color versions of one or more figures in this letter are available at https://doi.org/10.1109/LED.2021.3132415.

Digital Object Identifier 10.1109/LED.2021.3132415

0741-3106 © 2021 IEEE. Personal use is permitted, but republication/redistribution requires IEEE permission.
See https://www.ieee.org/publications/rights/index.html for more information.

Authorized licensed use limited to: Xiamen University. Downloaded on January 02,2022 at 01:00:54 UTC from IEEE Xplore. Restrictions apply.

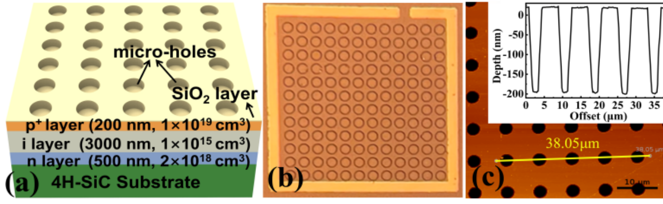

Fig. 1. (a) The schematic structure of 4H-SiC device with micro-hole array. (b) The top-view photograph of fabricated micro-hole array with p electrode. (c) Surface morphology of micro-holes with 3 μm in diameter measured by AFM and the corresponding cross-sectional profile shown in the inset.

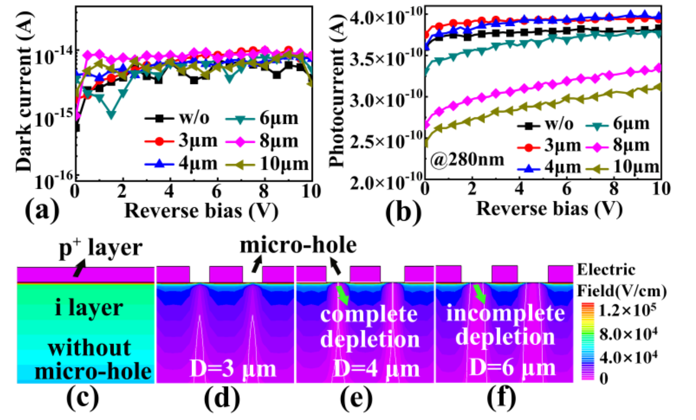

Fig. 2. The reverse current-voltage of devices with and without micro-hole (a) under dark on a log scale and (b) under the illumination of 280 nm on a linear scale. TCAD simulations of electric field intensity distribution in depletion region at 10 V bias for devices (c) without micro-hole, (d) with 3 μm micro-hole, (e) with 4 μm micro-hole and (f) with 6 μm micro-hole.

lifetime, Shockley-Read-Hall (SRH) recombination and for concentration and field dependent mobility models.

Firstly, a beveled mesa of device was processed by photoresist reflow technology to effectively suppress the edge breakdown of the device. Then, a standard photolithography process is used to obtain the micro-hole array patterns by using AZ5214E positive photoresist. Five kinds of micro-hole diameters (D = 3, 4, 6, 8, and 10 μm) were prepared, and the micro-hole spacing is fixed to 5 μm. Subsequently, the inductive coupled plasma (ICP) etching was performed with a gas flow rate of 30 sccm (CF_4)/5 sccm (O_2). The etching time was 250s, corresponding to a predicted etching depth of 210 ± 10 nm. Then, a lift-off process is applied to obtain the micro-hole array. Atomic force microscope (AFM) was employed to characterize the shape and size of the micro-holes as shown in Fig. 1(c). The micro-holes show a good uniformity and the etching depth of micro-holes is almost same as 220 nm, indicating that micro-holes are etched to the underlying i layer, which meet with the requirements of devices.

Then, an approximate 45-nm-thick SiO_2 was deposited, which is beneficial to reduce the surface dark current of the device and suppress the edge breakdown of micro-hole. Ti(40 nm)/Al(60 nm)/Ti(10 nm)/Au (100 nm) and Ti(5 nm)/Ni(200 nm)/Ti(5 nm)/Au (150 nm) metals were sputtered on the p^+ layer and the backside of n^+ substrate, respectively, followed by rapid thermal annealing in Ar ambient at 1000 °C for 2 min to form Ohmic contacts. As a final step, Ti(20 nm)/Au (300 nm) was sputtered as wire-bonding pad. For comparison, the traditional 4H-SiC p-i-n PDs without micro-holes were also fabricated by using the same process. Keithley 4200 analyzer was used to obtain the current-voltage (I-V) characteristics of devices. A Xenon lamp as the light source was connected with a monochromator for single wavelength selection to measure the spectral response.

III. Results and Discussion

Fig. 2(a) and (b) show the dark current and photocurrent characteristics of devices with and without micro-hole. The average dark currents of PDs were ultralow about 6×10^{-15} A in the reverse bias range of 0-10 V. The dark currents of device with micro-holes show no significant increase, which is attributed to the dark current effectively restrained by the oxide layer deposited on the micro-holes. Fig. 2(b) indicates that the photocurrents of devices with micro-holes (D = 3 and 4 μm) are larger than that without micro-holes, however, the photocurrents of devices with micro-holes (D = 6, 8, and 10 μm) have a significant decrease. This phenomenon that photocurrent increases first and then decreases as the micro-hole diameter increases, which is mainly due to the absorption layer at the micro-hole cannot be completely depleted when the micro-hole diameter is larger than a certain value (D $\geq$ 6 μm). Therefore, as the micro-hole diameter less than this certain critical value, the absorption layer at the micro-hole can be completely depleted, thus the photocurrents of the devices with micro-hole are significantly greater than the device without micro-hole.

Fig. 2(c)-(f) show electric field intensity distribution in depletion region of devices with and without micro-holes simulated by TCAD. The devices without micro-hole and with micro-holes (D = 3 and 4 μm) can be completely depleted at 10 V bias, so the photocurrents remain relatively stable with the increase of voltage. While the micro-hole diameter is larger than or equal to 6 μm, the absorption layer at micro-hole cannot be depleted completely in the horizontal direction, as shown in Fig. 2(f). Thus, the depletion region of the absorption layer will gradually become larger and the photocurrent will slowly increase with the increases of the reverse voltage.

The responsivity (R) and corresponding external quantum efficiency (η) can be calculated by the following formulas [22],

$$R = \frac{I_p}{P_{opt}} = \frac{I_{ph} - I_d}{P_{opt}} \quad (1)$$

$$\eta = \frac{1241R}{\lambda} \quad (2)$$

where I_{ph} and I_d represent the photocurrent and dark current of PDs, respectively. P_{opt} is the optical power in watts. The I_{ph} is four orders of magnitude larger than I_d for any PDs (I_{ph}-$I_d \approx I_{ph}$), therefore R depends linearly on I_{ph}. λ is the wavelength in nm.

Fig. 3(a) indicates that the spectral response and external quantum efficiency of the devices at 10 V bias. The device with 4 μm micro-hole exhibited a peak responsivity of 0.159 A/W at 290 nm (η = 68.1 %). Its peak responsivity and quantum efficiency are increased by 10.4 % and

Authorized licensed use limited to: Xiamen University. Downloaded on January 02,2022 at 01:00:54 UTC from IEEE Xplore. Restrictions apply.

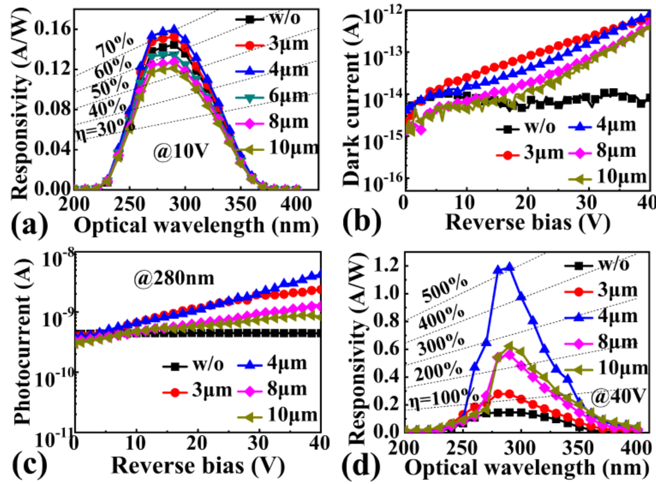

Fig. 3. (a) Spectral response of devices with and without micro-hole at 10 V bias. (b) Dark I-V and (c) photocurrent voltage characteristics at the bias from 0-40 V. (d) Spectral response of devices at 40 V bias.

6.5 %, respectively, compared to the device without micro-hole ($R = 0.144$ A/W and $\eta = 61.6$ %). The micro-hole area of device with 3 μm and 4 μm micro-hole are accounted for 7.7 % and 10.9 % of the single device area, respectively. Therefore, device with 4 μm micro-hole has a larger ratio of micro-hole area to device area than device with 3 μm micro-hole, resulting in more UV light directly absorbed by the i layer and improving the quantum efficiency (η). Nevertheless, it should be noted that the spectral responsivities of devices with micro-holes ($D = 6$, 8, and 10 μm) decreased because of the absorption layer at the micro-hole cannot be completely depleted. Although the photosensitive area has been increased and the absorption of the p^+ layer has also been reduced, there is no electric field in the middle area of the micro-hole and the photo-generated carriers cannot be separated, which leads to the decrease of spectral response.

As shown in Fig. 3(b) and Fig. 3(c), the dark current and photocurrent of devices without micro-hole remain stable at the bias range of 0-40 V. However, when the reverse bias is greater than 15 V, the dark current and photocurrent of the devices with micro-holes gradually increase. This phenomenon may be due to the local avalanche effect of the device with micro-hole. This effect can be explained that there is a higher electric field in the depletion region near the micro-hole arrays, which lead to electrons and holes could obtain higher kinetic energy, and collide with the crystal lattice of SiC, then generate a large number of electron-hole pairs. The local avalanche effect of the device with micro-holes leads to the increase of both dark current and photocurrent, and the ratio of photocurrent to dark current close to 10^4 when the reverse bias is 40 V. Fig. 3 (d) shows the spectral response of devices with micro-holes under 40 V bias. The peak responsivity and external quantum efficiency of the device with 4 μm micro-hole reach 1.19 A/W and 508 % at 40 V bias, which are 815 % and 819 % higher than that of the device without micro-hole respectively.

To further verify the local avalanche effect occurred in the absorption layer at the micro-holes, the electric field intensity at the micro-hole was simulated by TCAD. According to

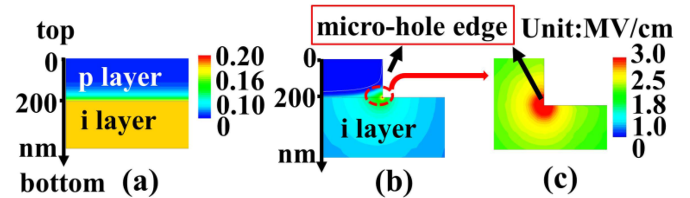

Fig. 4. The electric field intensity distribution diagrams of devices simulated by TCAD at 40 V bias (a) without micro-hole and (b) with micro-hole of 4 μm in diameter and 200 nm in depth. (c) Enlarged view of the micro-hole edge shown in Fig. 4 (b).

Fig. 4 (a), the maximum electric field intensity of the device without micro-hole is 0.2 MV/cm, which is less than the critical breakdown electric field of 4H-SiC (~3.0 MV/cm) [23]. As shown in Fig. 4 (b) and (c), the maximum electric field intensity of the device with diameter of 4 μm and depth of 200 nm micro-hole can arrive at 3.0 MV/cm, which is sufficient to induce local avalanche effect. Moreover, there are some regions in the micro-hole with such high electric field intensity, which is likely to cause avalanche breakdown.

As the reverse bias is increased to 40V, the depletion region does not expand, which means the micro-hole still cannot be completely depleted for device with micro-hole diameter larger than or equal to 6 μm. However, devices with micro-hole ($D = 3$ and 4 μm) can be completely depleted at the micro-holes. Moreover, device with 4 μm micro-hole has a larger micro-hole absorption area. The electric field intensity at the edge of the micro-hole has reached the condition of SiC avalanche breakdown, which can prove that the gain at 40V bias comes from the avalanche mechanism. Therefore, considering the change of depletion region and the electric field of the micro-hole edge, the device with 4 μm micro-hole can not only be completely depleted at the micro-hole, but also has adaptive electric field intensity at the edge of the micro-hole, which contributes to a highest responsivity and external quantum. These results indicate that the p-i-n devices with 4 μm micro-hole obtain a remarkable performance at a low voltage (~40 V).

In order to obtain large current gain, the fabricated p-i-n devices with micro-hole arrays require relative lower voltage, compared with the conventional APDs that usually operate at avalanche breakdown voltage of higher than 100 V. Besides, the gain of devices obtained at 40 V is reliable and repeatable. And the local avalanche at low voltage is easy to control without quenching circuit, and increases the lifetime of devices.

IV. Conclusion

In this letter, 4H-SiC p-i-n UV PDs with periodic micro-hole arrays are fabricated and measured. The 4H-SiC PDs exhibit an average dark current about 6.0×10^{-15} A in the reverse bias range of 0-10 V. Compared to device without micro-hole, the peak responsivity and corresponding external quantum efficiency of device with 4 μm micro-hole under 10 V bias are increased by 10.4 % and 6.5 %, respectively. As the bias increased to 40 V, the peak responsivity and external quantum efficiency increase by 815 % and 819 %, respectively. This research has a great significance to improve the application for weak UV detection.

Authorized licensed use limited to: Xiamen University. Downloaded on January 02,2022 at 01:00:54 UTC from IEEE Xplore. Restrictions apply.

References

[1] M. Kim, J.-H. Seo, U. Singisetti, and Z. Ma, "Recent advances in free-standing single crystalline wide band-gap semiconductors and their applications: GaN, SiC, ZnO, $\beta - Ga_2O_3$, and diamond," *J. Mater. Chem. C*, vol. 5, no. 33, pp. 8338–8354, 2017, doi: 10.1039/C7TC02221B.

[2] H. Chen, K. Liu, L. Hu, A. A. Al-Ghamdi, and X. Fang, "New concept ultraviolet photodetectors," *Mater. Today*, vol. 18, no. 9, pp. 493–502, Nov. 2015, doi: 10.1016/j.mattod.2015.06.001.

[3] Z. Alaie, S. M. Nejad, and M. H. Yousefi, "Recent advances in ultraviolet photodetectors," *Mater. Sci. Semicond. Process.*, vol. 29, pp. 16–55, Jan. 2015, doi: 10.1016/j.mssp.2014.02.054.

[4] A. R. Powell and L. B. Rowland, "SiC materials-progress, status, and potential roadblocks," *Proc. IEEE*, vol. 90, no. 6, pp. 942–955, Jun. 2002, doi: 10.1109/JPROC.2002.1021560.

[5] X. Chen, H. Zhu, J. Cai, and Z. Wu, "High-performance 4H-SiC-based ultraviolet p-i-n photodetector," *J. Appl. Phys.*, vol. 102, no. 2, Jul. 2007, Art. no. 024505, doi: 10.1063/1.2747213.

[6] F. Zhang, W. Yang, H. Huang, X. Chen, Z. Wu, H. Zhu, H. Qi, J. Yao, Z. Fan, and J. Shao, "High-performance 4H-SiC based metal-semiconductor-metal ultraviolet photodetectors with Al_2O_3/SiO_2 films," *Appl. Phys. Lett.*, vol. 92, no. 25, Jun. 2008, Art. no. 251102, doi: 10.1063/1.2949318.

[7] S. Hou, P.-E. Hellstrom, C.-M. Zetterling, and M. Ostling, "550 °C 4H-SiC p-i-n photodiode array with two-layer metallization," *IEEE Electron Device Lett.*, vol. 37, no. 12, pp. 1594–1596, Dec. 2016, doi: 10.1109/LED.2016.2618122.

[8] X. Zhou, T. Han, Y. Lv, J. Li, W. Lu, Y. Wang, X. Song, X. Tan, S. Liang, Z. Feng, and S. Cai, "Large-area 4H-SiC ultraviolet avalanche photodiodes based on variable-temperature reflow technique," *IEEE Electron Device Lett.*, vol. 39, no. 11, pp. 1724–1727, Nov. 2018, doi: 10.1109/LED.2018.2871798.

[9] C. Sun, X. Chen, R. Hong, X. Li, X. Xu, X. Chen, J. Cai, X.-A. Zhang, W. Cai, Z. Wu, and F. Zhang, "Enhancing the photoelectrical performance of graphene/4H-SiC/graphene detector by tuning a Schottky barrier by bias," *Appl. Phys. Lett.*, vol. 117, no. 7, Aug. 2020, Art. no. 071102, doi: 10.1063/5.0012566.

[10] K. Li, H. D. Liu, Q. Zhou, D. McIntosh, and J. C. Campbell, "SiC avalanche photodiode array with microlenses," *Opt. Exp.*, vol. 18, no. 11, pp. 11713–11719, May 2010, doi: 10.1364/OE.18.011713.

[11] T. Zhou, R. Xu, B. Ruan, Y. He, Z. Liang, and X. Wang, "Study on new method and mechanism of microcutting-etching of microlens array on 6H-SiC mold by combining single point diamond turning with ion beam etching," *J. Mater. Process. Technol.*, vol. 278, Apr. 2020, Art. no. 116510, doi: 10.1016/j.jmatprotec.2019.116510.

[12] X. Liu, L. Yu, S. Yang, Q. Chen, L. Wang, S. Juodkazis, and H. Sun, "Optical nanofabrication of concave microlens arrays," *Laser Photon. Rev.*, vol. 13, no. 5, May 2019, Art. no. 1800272, doi: 10.1002/lpor.201800272.

[13] Y. Hou, C. Sun, J. Wu, R. Hong, J. Cai, X. Chen, D. Lin, and Z. Wu, "Effect of epitaxial layer's thickness on spectral response of 4H-SiC p-i-n ultraviolet photodiodes," *Electron. Lett.*, vol. 55, no. 4, pp. 216–217, Feb. 2019, doi: 10.1049/el.2018.8035.

[14] N. Naderi and M. R. Hashim, "Porous-shaped silicon carbide ultraviolet photodetectors on porous silicon substrates," *J. Alloys Compounds*, vol. 552, pp. 356–362, Mar. 2013, doi: 10.1016/j.jallcom.2012.11.085.

[15] T. Zhu, Y. Liu, T. Ding, W. Y. Fu, J. Jarman, C. X. Ren, R. V. Kumar, and R. A. Oliver, "Wafer-scale fabrication of non-polar mesoporous GaN distributed Bragg reflectors via electrochemical porosification," *Sci. Rep.*, vol. 7, no. 1, Mar. 2017, Art. no. 45344, doi: 10.1038/srep45344.

[16] R. Yu, G. Wang, Y. Shao, Y. Wu, S. Wang, G. Lian, B. Zhang, H. Hu, L. Liu, L. Zhang, and X. Hao, "From bulk to porous GaN crystal: Precise structural control and its application in ultraviolet photodetectors," *J. Mater. Chem. C*, vol. 7, no. 45, pp. 14116–14122, Nov. 2019, doi: 10.1039/C9TC04820K.

[17] X. Zhangyang, L. Liu, Z. Lv, F. Lu, and J. Tian, "Comparative analysis of light trapping GaN nanohole and nanorod arrays for UV detectors," *J. Nanoparticle Res.*, vol. 22, no. 8, p. 243, Aug. 2020, doi: 10.1007/s11051-020-04972-x.

[18] H. Zheng, Y. Jiang, S. Yang, Y. Zhang, X. Yan, J. Hu, Y. Shi, and B. Zou, "ZnO nanorods array as light absorption antenna for high-gain UV photodetectors," *J. Alloys Compounds*, vol. 812, Jan. 2020, Art. no. 152158, doi: 10.1016/j.jallcom.2019.152158.

[19] G.-Y. Lai, D. P. Kumar, and Z. Pei, "Periodic nano/micro-hole array silicon solar cell," *Nanosc. Res. Lett.*, vol. 9, no. 1, p. 654, Dec. 2014, doi: 10.1186/1556-276X-9-654.

[20] Y.-A. Chang, Z.-Y. Li, H.-C. Kuo, T.-C. Lu, S.-F. Yang, L.-W. Lai, L.-H. Lai, and S.-C. Wang, "Efficiency improvement of single-junction InGaP solar cells fabricated by a novel micro-hole array surface texture process," *Semicond. Sci. Technol.*, vol. 24, no. 8, Jul. 2009, Art. no. 085007, doi: 10.1088/0268-1242/24/8/085007.

[21] *ATHENA/ATLAS User's Manual*, SILVACO Internaional, Santa Clara, CA, USA, 1998. [Online]. Available: http://www.silvaco.com

[22] M. Razeghi and A. Rogalski, "Semiconductor ultraviolet detectors," *J. Appl. Phys.*, vol. 79, pp. 7433–7473, Jan. 1996, doi: 10.1063/1.362677.

[23] A. O. Konstantinov, Q. Wahab, N. Nordell, and U. Lindefelt, "Ionization rates and critical fields in 4H silicon carbide," *Appl. Phys. Lett.*, vol. 71, no. 1, pp. 90–92, Jul. 1997, doi: 10.1063/1.119478.

Authorized licensed use limited to: Xiamen University. Downloaded on January 02,2022 at 01:00:54 UTC from IEEE Xplore. Restrictions apply.